Current Biology

Pattern and Component Motion Responses in Mouse Visual Cortical Areas

Highlights

- Five different visual areas in the mouse were investigated for responses to plaids

- Mouse visual cortex cells respond in diverse ways to gratings and plaids

- Areas LM and RL contain small proportions of pattern cells; V1, AL, and AM do not

- LM and RL may constitute a dorsal, motion-sensitive stream in the mouse

Authors

Ashley L. Juavinett, Edward M. Callaway

Correspondence

callaway@salk.edu

In Brief

Juavinett et al. expand on the growing interest of the mouse as a model for visual neuroscience, demonstrating that cells in two areas of mouse visual cortex can compute the global motion of a plaid. The report of these pattern direction cells in areas LM and RL, but not V1, AL, or AM, further delineates dorsal and ventral streams in the mouse.

CrossMark

CellPress

Pattern and Component Motion Responses in Mouse Visual Cortical Areas

Ashley L. Juavinett[1,2] and Edward M. Callaway[1,2,*]
[1]The Salk Institute for Biological Studies, La Jolla, CA 92037, USA
[2]Neurosciences Graduate Program, University of California San Diego, La Jolla, CA 92093, USA
*Correspondence: callaway@salk.edu
http://dx.doi.org/10.1016/j.cub.2015.05.028

SUMMARY

Spanning about 9 mm^2 of the posterior cortex surface, the mouse's small but organized visual cortex has recently gained attention for its surprising sophistication and experimental tractability [1–3]. Though it lacks the highly ordered orientation columns of primates [4], mouse visual cortex is organized retinotopically [5] and contains at least ten extrastriate areas that likely integrate more complex visual features via dorsal and ventral streams of processing [6–14]. Extending our understanding of visual perception to the mouse model is justified by the evolving ability to interrogate specific neural circuits using genetic and molecular techniques [15, 16]. In order to probe the functional properties of the putative mouse dorsal stream, we used moving plaids, which demonstrate differences between cells that identify local motion (component cells) and those that integrate global motion of the plaid (pattern cells; Figure 1A; [17]). In primates, there are sparse pattern cell responses in primate V1 [18, 19], but many more in higher-order regions; 25%–30% of cells in MT [17] and 40%–60% in MST [20] are pattern direction selective. We present evidence that mice have small numbers of pattern cells in areas LM and RL, while V1, AL, and AM are largely component-like. Although the proportion of pattern cells is smaller in mouse visual cortex than in primate MT, this study provides evidence that the organization of the mouse visual system shares important similarities to that of primates and opens the possibility of using mice to probe motion computation mechanisms.

RESULTS

In an effort to extend our understanding of visual information processing in the rodent system so that we may capitalize on experimental advantages, we have used a common stimulus from primate research to probe motion processing in the mouse model. We used intrinsic signal imaging followed by two-photon calcium imaging in layer 2/3 of 2- to 4-month-old anesthetized mice to record responses to grating and plaid stimuli in primary visual cortex (V1) and four extrastriate areas (lateromedial [LM], anterolateral [AL], rostrolateral [RL], and anteromedial [AM]).

Although visual areas in the mouse are quite small, borders between areas can be functionally mapped using intrinsic signal optical imaging [21], ideally with a periodic stimulus [13, 22]. We therefore first used intrinsic signal optical imaging during the presentation of a full-field continuous contrasting-reversing checkerboard bar in altitude and azimuth directions to semi-automatically determine borders between visual areas (Figures 1C and 1D; [7, 13, 21, 22]). With this method, functional maps can be accurately computed for each mouse, allowing for individual identification of visual area borders, important due to small area size and slight differences between mice [13]. Using these functional maps overlaid on blood vessel patterns as a guide, we then loaded Oregon Green Bapta (OGB) into layer 2/3 of the targeted area (Figure 1E).

Moving plaids consist of two drifting gratings combined additively and offset by an angle (Figure 1A; [23]). In primates, visual area medial temporal (MT)/V5 contains cells that respond to the global motion of the plaid, termed "pattern" or "pattern direction-selective (PDS)" cells (Figure 1B; [17]). Other cells, present in both V1 and MT, encode the individual gratings of the plaid and are termed "component" or "component direction-selective (CDS)" cells (Figure 1B). Thus, after OGB loading, we investigated the responses of cells to full-screen 100% contrast drifting gratings and 120° plaids (50% contrast for each grating) moving in 12 different directions to identify cells that responded to either the individual, component motions of the plaid or the global, perceived motion of the plaid (Supplemental Experimental Procedures; [17]).

We imaged thousands of cells in V1, LM, AL, RL, and AM in 34 different animals (Table S1). Of these cells, 15%–25% (depending on visual area) were responsive ($\Delta F/F > 6\%$) and reliable (determined by a d′ metric [7]; Supplemental Experimental Procedures) to at least one type of stimulus (LM: 12.8% [588 out of 4,577]; AL: 13.4% [508 out of 3,970]; RL: 17.6% [921 out of 5,232]; V1: 25% [1,192 out of 4,743]; Table S1), consistent with previous studies investigating visual responses in these areas in both awake [8] and anesthetized [7] mice. Only cells meeting the responsive and reliable criteria for at least one stimulus were included in further analysis to determine stimulus preferences.

We then looked to see whether these cells responded to gratings, plaids, or both. While some cells were responsive and reliable to both stimuli, certain cells responded only to the simple drifting gratings, and another subset responded solely to plaids (Figure 2A). Across areas, there were differences in
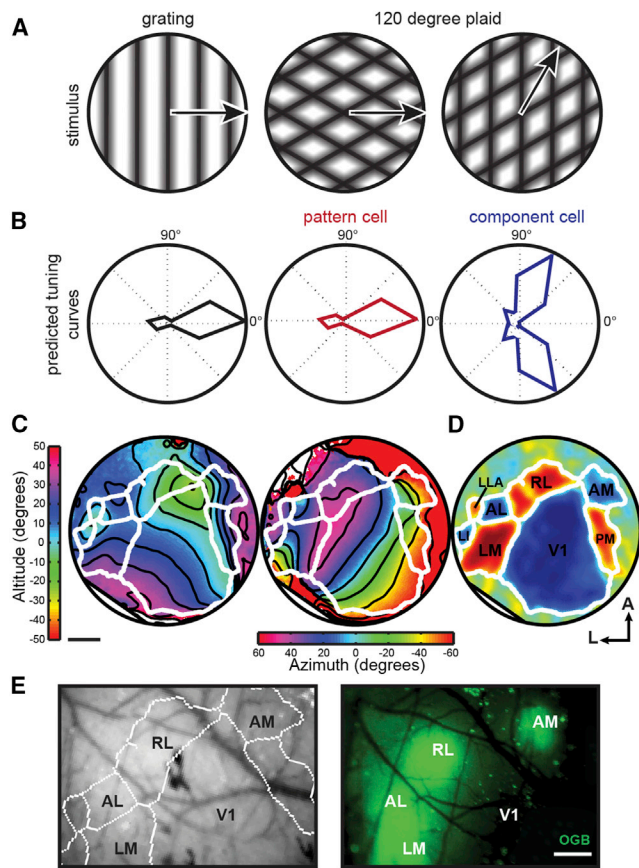
Figure 1. Classifying Pattern-like and Component-like Responses to Plaid Stimuli in Multiple Visual Areas

(A) Schematic of sinusoidal gratings and plaids. Left plaid has same pattern motion as grating; right plaid has a different pattern motion but contains the rightward-moving grating component.

(B) Left: hypothetical response to grating. Center and right: generated predictions for pattern and component tuning curves in response to plaids. The pattern response is identical to the DS cell response to the grating, whereas the component response has two lobes to account for the two directions of the plaid (one direction shown in A) that contain the preferred component.

(C) Sample azimuth and altitude intrinsic signal imaging (ISI) data from one animal with five repeats of the stimulus. Contour lines are overlaid in black; area borders as determined by semi-automatic border analysis are overlaid in white. The scale bar represents 500 μm.

(D) Visual field sign computed as the sine of the difference in the angle between the horizontal and vertical map gradients. Regions with a red visual field sign have a non-mirror representation of visual space, whereas areas in blue have a mirror representation. Regions that are not clearly red or blue lack retinotopic structure. Identified visual areas are labeled.

(E) Left: visual area borders generated from (C) and (D) overlaid on blood vessel picture. Right: subsequent OGB loading into targeted areas. The scale bar represents 500 μm.

the proportions of cells that were responsive to each stimulus (Figure 2B); while 38%–46% of responsive and reliable cells in V1, LM, AL, and AM responded to both gratings and plaids, 60% (553 out of 921) of cells in RL responded to both. AL had the highest proportion of cells responsive only to gratings (43%; 218 out of 508), while V1 and RL had the lowest (22% and 24%, respectively). A relatively high proportion (37%; 441
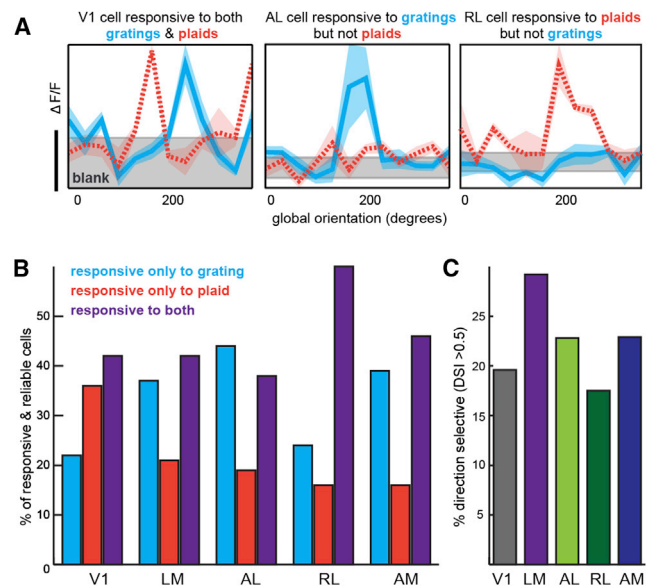

Figure 2. Sample Tuning Curves and Distribution of Responses to Gratings and Plaids

(A) Example tuning curves from V1, AL, and RL, demonstrating diverse visual responses to grating or plaid stimuli. Left: V1 cell responds above baseline (gray) to both gratings (cyan) and plaids (orange dashed line). Center: AL cell responds to only gratings. Right: RL cell responds only to plaids. Shaded area around curves represents SEM; gray baseline shaded area is the mean ΔF/F ± SEM. The scale bar corresponds to 5% ΔF/F.

(B) Percent of responsive and reliable cells in each area that responded to only drifting gratings, only 120° plaids, or both.

(C) Percent of cells that were DS (DSI > 0.5), taken out of the total number of responsive and reliable cells.

See also Figure S1.

out of 1,192) of cells in V1 responded exclusively to plaids and not gratings (Figure S1).

Only cells that respond to both gratings and plaids can be assessed for their preference for pattern or component motion [17]. Furthermore, only direction-selective (DS) cells can be pattern or component motion DS (by the standard definition). Therefore, the subset of cells that were responsive and reliable to both gratings and plaids were then tested for direction selectivity. In V1, about 19.6% of these cells were DS (determined by standard metrics where direction selectivity index [DSI] > 0.5), whereas 22.8%–29.2% of cells in LM, AL, and AM were DS, consistent with previous reports (Figure 2C; [7]). We found a relatively low percentage of DS cells in RL (17.5%), possibly because the stimulus was not optimized for the high-temporal and low-spatial frequency preferences of this area [7]. The cells that were responsive and reliable to both gratings and plaids and were also DS were included in the subsequent component and pattern correlation analyses.

In order to characterize cells as pattern, component, or unclassified, we generated predicted tuning curves for pattern and component cells from the grating responses for each cell, as previously described (Figure 1B; [17]). The two predicted tuning curves were then correlated with the responses to the plaid stimulus to give two correlation values for each cell, Rc and Rp. These correlation values were then normalized with a
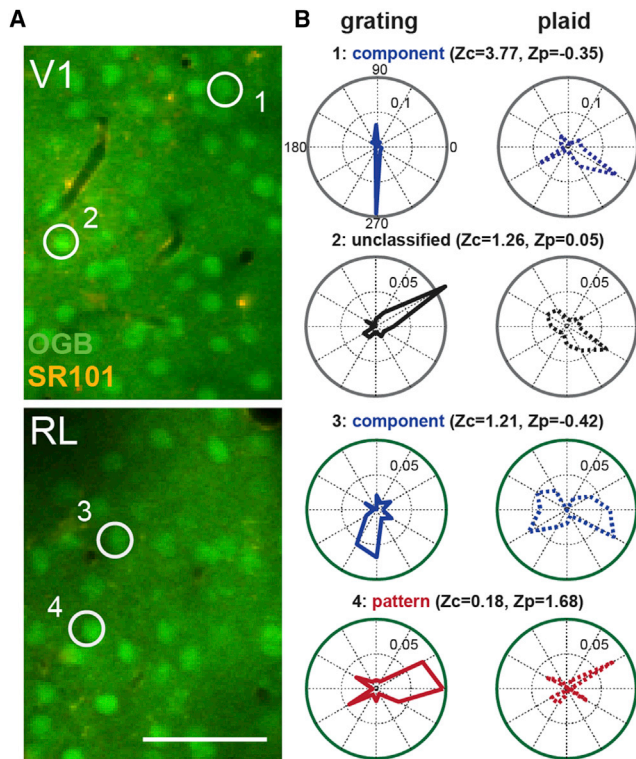
A

B

Figure 3. OGB and SR101 Loading in V1 and RL with Cell Examples

(A) Example two-photon data from V1 (top) and RL (bottom) with OGB (neurons) and SR101 (glia) loading. The scale bar represents 50 μm.

(B) Sample tuning curves from component, unclassified, and pattern cells. Z-scored component (Zc) and pattern (Zp) values are given for each cell. Numbered circles in the images (A) indicate neurons that correspond to the numbered tuning curves (B). Values within polar plots indicate ΔF/F scale to the inner dotted ring of each plot.

Fisher r-to-Z transformation to permit the calculation of a difference between correlation values, generating Z pattern (Zp) and Z component (Zc; [24]). A significantly high Zp value classifies the cell as PDS, whereas a high Zc value classifies it as CDS. Cells with correlation values that were not significantly different from each other or zero were deemed unclassified.

Cell responses to the stimulus set of grating and plaids varied on a continuum from PDS to CDS responses. Some cells were CDS and had a very clear bi-lobed tuning curve in response to plaids because a plaid moving in two different directions contained the grating component that the cell preferred (Figure 3B). Alternatively, several cells responded to just one plaid with the same global motion as its preferred grating (Figure 3B) and were therefore PDS.

Across areas, the proportion of PDS, CDS, and unclassified cells differed: LM and RL were the only areas containing cells exhibiting pattern direction selectivity (Figure 4A). Approximately 5.8% of cells in LM were PDS (4 out of 69), while 8.3% (8 out of 96) of cells in RL were PDS. V1 had no PDS cells, but 30.1% (25 out of 83) of the cells included in the analysis (as described above) were classified as CDS. Area AL was marked by the highest percentage of CDS cells (39.5%, 15 out of 38), with many cells that had well-tuned responses to both gratings and plaids.

Lastly, AM did not have any PDS cells, but 30.8% (8 out of 26) were clearly CDS. In addition, we conducted a subset of experiments with awake-behaving mice, but this did not drastically change the proportion of pattern cells in RL (Figure S1). Each area had a set of cells that did not significantly correlate with a CDS or PDS prediction, though often these were qualitatively component- or pattern-like (see cell example 2 in Figure 3B).

In addition to cells that are clearly classified as CDS or PDS, the unclassified cells have biases in their responses that can be observed as the difference between Zc and Zp. We therefore also computed a component index for each cell by subtracting Zp from Zc to obtain a more graded measure of how the cell responses differed across areas (Figure 4B). The distributions of Zc − Zp values as well as their means differed between the populations of cells sampled in each area, with AL being the most component-like and RL the most pattern-like. Specifically, the mean Zc − Zp value was highest (most component-like) for area AL (1.53 ± 0.22, mean ± SEM) and was lowest (most pattern-like) for LM (1.05 ± 0.18) and RL (0.97 ± 0.18). The mean values for areas V1 and AM were intermediate (1.32 ± 0.17 and 1.37 ± 0.24, respectively).

When proportions of CDS, unclassified, and PDS cells were compared across areas, there were clear significant differences. The number of PDS, unclassified, and CDS cells was significantly different between V1 and LM ($p < .05$), V1 and RL ($p < .01$), and AL and RL ($p < .05$), as determined by a Fisher's exact test (Figure 4B; these differences remain significant when corrected for multiple comparisons with a Benjamini-Hochberg procedure; false discovery rate [FDR] = 0.2). While the number of PDS cells was significantly different in RL and LM when compared to V1, AL and AM were not different from V1 (Figure 4B).

DISCUSSION

While mice have been shown to have multiple visual cortical areas with functional preferences, it is unknown whether these areas generate higher-order functional specializations like those in the primate visual system. In particular, it is unknown whether mice compute complex visual movement akin to primates. To further assess the potential of mouse visual system for elucidating circuit mechanisms of complex behaviors, we turned to the plaid stimulus, which has proved useful for visual neuroscience in cats and monkeys for the past 30 years [17].

Here, we present evidence that mice have cells that can compute pattern motion and that in the five areas that were tested, these cells are found only in visual areas LM and RL. Meanwhile, mouse V1, AL, and AM do not have any evidence of PDS responses. We found CDS responses in all of the visual areas we tested, suggesting that this is a more fundamental computation that each area can complete. It should be noted that our experiments were restricted to layers 2/3 of cortex, and it is possible that there are laminar differences in responses to plaids. In essence, V1, AL, and AM appear to be "blind" to the global motion of the stimulus, even though many cells in these regions responded in some way to the plaid stimulus. On the contrary, proper processing of moving plaids to provide accurate information about the global movement of the stimulus is effectively completed in specific cells of areas LM and RL, which
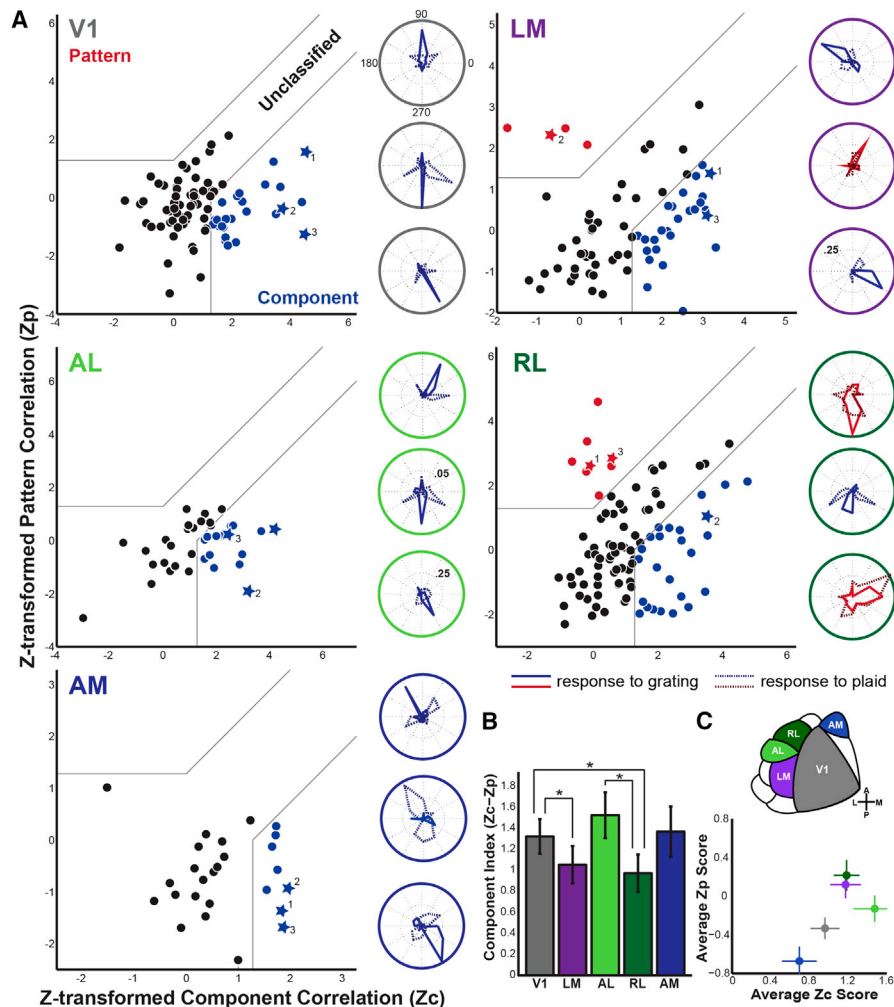
Figure 4. Pattern and Component Correlation Plots by Visual Area

(A) Z-transformed pattern (Zp) versus component (Zc) correlation for V1, LM, AL, RL, and AM. Cells with tuning curves plotted to the right are denoted as stars in the scatterplots. All cells are colored according to classification (red indicates pattern, black indicates unclassified, and blue indicates component). Gray lines divide plots into areas that are significantly pattern direction selective (PDS), unclassified, or component direction selective (CDS). Outside ring of polar plots is color coded for each visual area. Values within polar plots indicate ΔF/F scale to the inner dotted ring of each plot; inner ring is 10% ΔF/F unless otherwise noted.

(B) Mean component index (Zc − Zp) by visual area. Error bars show SEM. *p < 0.05 (Fisher's exact test).

(C) Top: schematic of mouse visual areas. Bottom: average Zc score plotted against the average Zp score for each visual area. Error bars show SEM. The visual area corresponding to each point is indicated by colors in top area schematic.

For further characterization of these data, see Figure S2.

may constitute a dorsal, movement-sensitive pathway in the mouse [7, 8]. This integration is essential for correctly computing optic flow and effectively initiating movement.

Although RL contains a much lower percentage of pattern cells than seen in primate MT, it is worth noting that it shares other important similarities with MT. Anatomical studies have suggested that RL is a node of the mouse dorsal stream [10]. Like MT, RL receives direct input from V1 as well as V2/LM [9, 10], and both MT and RL have a bias toward the lower visual field in their retinotopic organization [13, 25]. RL projects to barrel and whisker motor cortex as well as deep layers of the superior colliculus [11], suggesting it is involved in navigation and visually guided orienting. In addition, RL exhibits multisensory enhancement for visual and tactile stimuli [26].

Despite these similarities, there is a marked difference in the direction selectivity of MT and RL—almost every cell in MT is DS [27, 28], whereas about 18%–27% of RL cells are DS [7]. Shown here, RL is the most pattern-selective area in the mouse, with 8% of DS cells responding to pattern motion. While this is a small proportion compared to primate MT, it is unlikely these were recorded by chance in light of the differences between RL and V1. In addition, because the stimulus was not optimized for each individual neuron as in single-cell electrophysiology, it is likely that we have under-sampled the number of responsive and potentially pattern-selective cells. Future studies will need to address the known anatomical and functional markers of MT, such as surround suppression, binocular disparity, and DS V1 inputs [29] in

order to fully test the validity of the comparison between RL and MT.

Previous studies have shown that mice can compute the global motion of a stimulus but have not explored the mechanistic basis for this behavior [30]. The presence of PDS cells in the mouse suggests that they achieve this computation in a similar way to primates, but with fewer cells overall. It is possible that the downstream consequences of pattern integration, such as motor output for head or body orienting, are achieved with fewer cells that can compute such motion, or that these computations are completed in networks rather than individual cells. Our observation that many cells respond to plaid stimuli (Figure 2), often in ways that did not conform to a CDS or PDS prediction (Figure 4), suggests that mice might employ a novel computation to perform pattern motion integration and inform downstream behavioral output. This speculation is further supported by the fact that many cells, even in V1, responded significantly to plaids, but not gratings (Figure S1). Such cells might support sensation of global motion differently than in primates, obviating the need for large numbers of PDS cells. Alternatively, these cells might prefer spatial frequencies that were present in the plaids, but not the gratings.

Evidence for pattern direction selectivity in LM and RL, but not V1, AL, or AM, can build on current anatomical frameworks to inform proper parsing of dorsal and ventral streams in the mouse. While most of the focus has been on pattern selectivity, we are intrigued by the high proportion of component cells in AL. Previous studies have suggested that AL is a gateway to the dorsal stream [7, 9], yet the present work suggests that it is not involved in plaid motion integration, a prominent characteristic of dorsal stream function. On the other hand, anatomical data have led other researchers to position LM as part of the ventral stream [9, 10], although it clearly projects to both dorsal and ventral targets. Indeed, the rationale used to place LM in the ventral stream places V1 there as well [10]. Our past investigation into the spatial and temporal frequency preferences of LM [7] and present data for plaid motion processing suggest that LM is involved in the dorsal stream as well and may be akin to primate V2 in this regard [22, 31]. Further functional studies of these areas with more diverse and complex visual stimuli, including objects, figure-ground separation, colors, etc., will be necessary to explicate functional differences and draw a clear hierarchy between these regions.

As there is a significant gain in response intensity with movement [32, 33], and other researchers have posited that plaid motion integration may change with brain state ([34], but see [35]), we ran a subset of experiments in awake animals but did not see a striking difference in the proportion of pattern cells (Figure S1). Although preliminary, this suggests that plaid motion integration does not depend on the state of the animal [35].

Our work here provides a basis to test the nuances of complex motion perception in mammalian visual systems and further unravels the function of higher-order mouse cortex. The demonstration of pattern motion-selective cells in genetically tractable mice, where specific cell types can be selectively manipulated [15], opens the door to studies probing the neural circuit mechanisms that underlie the production of pattern motion cells in higher-order visual areas from their component motion-selective V1 inputs. The use of single-cell monosynaptic tracing with the rabies virus [36, 37] in conjunction with genetically encoded calcium indicators could be a fruitful way to understand which cells provide inputs to pattern cells and how and when these inputs are combined [38, 39]. Already, various groups have capitalized on the methodological advantages afforded by the mouse model to address circuit-level questions of visual perception [40–42]; our work provides a necessary basis for similar future studies. The presence of pattern cells in mouse visual cortex suggests that questions regarding the cell types and connectivity motifs that underlie pattern motion computation can indeed be investigated in the mouse model.

SUPPLEMENTAL INFORMATION

Supplemental Information includes Supplemental Experimental Procedures, two figures, and one table and can be found with this article online at http://dx.doi.org/10.1016/j.cub.2015.05.028.

AUTHOR CONTRIBUTIONS

A.L.J. and E.M.C. designed experiments. A.L.J. conducted experiments and analyzed data. A.L.J. and E.M.C. wrote the manuscript.

ACKNOWLEDGMENTS

REFERENCES

1. Glickfeld, L.L., Reid, R.C., and Andermann, M.L. (2014). A mouse model of higher visual cortical function. Curr. Opin. Neurobiol. 24, 28–33.

2. Carandini, M., and Churchland, A.K. (2013). Probing perceptual decisions in rodents. Nat. Neurosci. 16, 824–831.

3. Hübener, M. (2003). Mouse visual cortex. Curr. Opin. Neurobiol. 13, 413–420.

4. Ohki, K., Chung, S., Ch'ng, Y.H., Kara, P., and Reid, R.C. (2005). Functional imaging with cellular resolution reveals precise micro-architecture in visual cortex. Nature 433, 597–603.

5. Wagor, E., Mangini, N.J., and Pearlman, A.L. (1980). Retinotopic organization of striate and extrastriate visual cortex in the mouse. J. Comp. Neurol. 193, 187–202.

6. Wang, Q., and Burkhalter, A. (2007). Area map of mouse visual cortex. J. Comp. Neurol. 502, 339–357.

7. Marshel, J.H., Garrett, M.E., Nauhaus, I., and Callaway, E.M. (2011). Functional specialization of seven mouse visual cortical areas. Neuron 72, 1040–1054.

8. Andermann, M.L., Kerlin, A.M., Roumis, D.K., Glickfeld, L.L., and Reid, R.C. (2011). Functional specialization of mouse higher visual cortical areas. Neuron 72, 1025–1039.

9. Wang, Q., Gao, E., and Burkhalter, A. (2011). Gateways of ventral and dorsal streams in mouse visual cortex. J. Neurosci. 31, 1905–1918.

10. Wang, Q., Sporns, O., and Burkhalter, A. (2012). Network analysis of corticocortical connections reveals ventral and dorsal processing streams in mouse visual cortex. J. Neurosci. 32, 4386–4399.

11. Wang, Q., and Burkhalter, A. (2013). Stream-related preferences of inputs to the superior colliculus from areas of dorsal and ventral streams of mouse visual cortex. J. Neurosci. *33*, 1696–1705.

12. Roth, M.M., Helmchen, F., and Kampa, B.M. (2012). Distinct functional properties of primary and posteromedial visual area of mouse neocortex. J. Neurosci. *32*, 9716–9726.

13. Garrett, M.E., Nauhaus, I., Marshel, J.H., and Callaway, E.M. (2014). Topography and areal organization of mouse visual cortex. J. Neurosci. *34*, 12587–12600.

14. Polack, P.O., and Contreras, D. (2012). Long-range parallel processing and local recurrent activity in the visual cortex of the mouse. J. Neurosci. *32*, 11120–11131.

15. Luo, L., Callaway, E.M., and Svoboda, K. (2008). Genetic dissection of neural circuits. Neuron *57*, 634–660.

16. Callaway, E.M. (2005). A molecular and genetic arsenal for systems neuroscience. Trends Neurosci. *28*, 196–201.

17. Movshon, J.A., Adelson, E.H., Gizzi, M.S., and Newsome, W.T. (1985). The analysis of moving visual patterns. In Pattern Recognition Mechanisms, C. Chagas, R. Gattass, and C. Gross, eds. (Academia Scientiarum Scripta), pp. 117–151.

18. Tinsley, C.J., Webb, B.S., Barraclough, N.E., Vincent, C.J., Parker, A., and Derrington, A.M. (2003). The nature of V1 neural responses to 2D moving patterns depends on receptive-field structure in the marmoset monkey. J. Neurophysiol. *90*, 930–937.

19. Khawaja, F.A., Tsui, J.M.G., and Pack, C.C. (2009). Pattern motion selectivity of spiking outputs and local field potentials in macaque visual cortex. J. Neurosci. *29*, 13702–13709.

20. Khawaja, F.A., Liu, L.D., and Pack, C.C. (2013). Responses of MST neurons to plaid stimuli. J. Neurophysiol. *110*, 63–74.

21. Schuett, S., Bonhoeffer, T., and Hübener, M. (2002). Mapping retinotopic structure in mouse visual cortex with optical imaging. J. Neurosci. *22*, 6549–6559.

22. Kalatsky, V.A., and Stryker, M.P. (2003). New paradigm for optical imaging: temporally encoded maps of intrinsic signal. Neuron *38*, 529–545.

23. Adelson, E.H., and Movshon, J.A. (1982). Phenomenal coherence of moving visual patterns. Nature *300*, 523–525.

24. Smith, M.A., Majaj, N.J., and Movshon, J.A. (2005). Dynamics of motion signaling by neurons in macaque area MT. Nat. Neurosci. *8*, 220–228.

25. Maunsell, J.H., and Newsome, W.T. (1987). Visual processing in monkey extrastriate cortex. Annu. Rev. Neurosci. *10*, 363–401.

26. Olcese, U., Iurilli, G., and Medini, P. (2013). Cellular and synaptic architecture of multisensory integration in the mouse neocortex. Neuron *79*, 579–593.

27. Albright, T.D. (1984). Direction and orientation selectivity of neurons in visual area MT of the macaque. J. Neurophysiol. *52*, 1106–1130.

28. Dubner, R., and Zeki, S.M. (1971). Response properties and receptive fields of cells in an anatomically defined region of the superior temporal sulcus in the monkey. Brain Res. *35*, 528–532.

29. Born, R.T., and Bradley, D.C. (2005). Structure and function of visual area MT. Annu. Rev. Neurosci. *28*, 157–189.

30. Douglas, R.M., Neve, A., Quittenbaum, J.P., Alam, N.M., and Prusky, G.T. (2006). Perception of visual motion coherence by rats and mice. Vision Res. *46*, 2842–2847.

31. Rosa, M.G., and Krubitzer, L.A. (1999). The evolution of visual cortex: where is V2? Trends Neurosci. *22*, 242–248.

32. Niell, C.M., and Stryker, M.P. (2010). Modulation of visual responses by behavioral state in mouse visual cortex. Neuron *65*, 472–479.

33. Fu, Y., Tucciarone, J.M., Espinosa, J.S., Sheng, N., Darcy, D.P., Nicoll, R.A., Huang, Z.J., and Stryker, M.P. (2014). A cortical circuit for gain control by behavioral state. Cell *156*, 1139–1152.

34. Pack, C.C., Berezovskii, V.K., and Born, R.T. (2001). Dynamic properties of neurons in cortical area MT in alert and anaesthetized macaque monkeys. Nature *414*, 905–908.

35. Movshon, J.A., Albright, T.D., Stoner, G.R., Majaj, N.J., and Smith, M.A. (2003). Cortical responses to visual motion in alert and anesthetized monkeys. Nat. Neurosci. *6*, 3, author reply 3–4.

36. Wickersham, I.R., Lyon, D.C., Barnard, R.J.O., Mori, T., Finke, S., Conzelmann, K.-K., Young, J.A.T., and Callaway, E.M. (2007). Monosynaptic restriction of transsynaptic tracing from single, genetically targeted neurons. Neuron *53*, 639–647.

37. Marshel, J.H., Mori, T., Nielsen, K.J., and Callaway, E.M. (2010). Targeting single neuronal networks for gene expression and cell labeling in vivo. Neuron *67*, 562–574.

38. Thiele, A., and Stoner, G. (2003). Neuronal synchrony does not correlate with motion coherence in cortical area MT. Nature *421*, 366–370.

39. Movshon, J.A., and Newsome, W.T. (1996). Visual response properties of striate cortical neurons projecting to area MT in macaque monkeys. J. Neurosci. *16*, 7733–7741.

40. Nienborg, H., Hasenstaub, A., Nauhaus, I., Taniguchi, H., Huang, Z.J., and Callaway, E.M. (2013). Contrast dependence and differential contributions from somatostatin- and parvalbumin-expressing neurons to spatial integration in mouse V1. J. Neurosci. *33*, 11145–11154.

41. Cruz-Martín, A., El-Danaf, R.N., Osakada, F., Sriram, B., Dhande, O.S., Nguyen, P.L., Callaway, E.M., Ghosh, A., and Huberman, A.D. (2014). A dedicated circuit links direction-selective retinal ganglion cells to the primary visual cortex. Nature *507*, 358–361.

42. Lien, A.D., and Scanziani, M. (2013). Tuned thalamic excitation is amplified by visual cortical circuits. Nat. Neurosci. *16*, 1315–1323.